



Aerial Survey Robotics in Extreme Environments: Mapping Volcanic CO₂ Emissions With Flocking UAVs

John Ericksen^{1*}, G. Matthew Fricke^{1,2}, Scott Nowicki^{3,4}, Tobias P. Fischer³, Julie C. Hayes¹, Karissa Rosenberger³, Samantha R. Wolf³, Rafael Fierro⁵ and Melanie E. Moses^{1,6,7}

¹Computer Science Department, University of New Mexico, Albuquerque, NM, United States, ²Center for Advanced Research Computing, University of New Mexico, Albuquerque, NM, United States, ³Department of Earth and Planetary Sciences, University of New Mexico, Albuquerque, NM, United States, ⁴NV5, Albuquerque, NM, United States, ⁵Department of Electrical and Computer Engineering, University of New Mexico, Albuquerque, NM, United States, ⁶Biology Department, University of New Mexico, Albuquerque, NM, United States, ⁷Santa Fe Institute, Santa Fe, NM, United States

We present methods for autonomous collaborative surveying of volcanic CO₂ emissions using aerial robots. CO₂ is a useful predictor of volcanic eruptions and an influential greenhouse gas. However, current CO₂ mapping methods are hazardous and inefficient, as a result, only a small fraction of CO₂ emitting volcanoes have been surveyed. We develop algorithms and a platform to measure volcanic CO₂ emissions. The Dragonfly Unpiloted Aerial Vehicle (UAV) platform is capable of long-duration CO₂ collection flights in harsh environments. We implement two survey algorithms on teams of Dragonfly robots and demonstrate that they effectively map gas emissions and locate the highest gas concentrations. Our experiments culminate in a successful field test of collaborative rasterization and gradient descent algorithms in a challenging real-world environment at the edge of the Valles Caldera supervolcano. Both algorithms treat multiple flocking UAVs as a distributed flexible instrument. Simultaneous sensing in multiple UAVs gives scientists greater confidence in estimates of gas concentrations and the locations of sources of those emissions. These methods are also applicable to a range of other airborne concentration mapping tasks, such as pipeline leak detection and contaminant localization.

Keywords: coverage, flocking, robotics, unmanned aerial vehicle, CO₂, volcanic

1 INTRODUCTION

Distributed mobile sensing has many application areas, such as monitoring of industrial gas leaks, hazardous material releases, and agricultural monitoring (Rossi et al., 2014; Gomez and Purdie, 2016; Radoglou-Grammatikis et al., 2020).¹ Often the materials we are interested in sensing can only be directly sampled, as the signal of CO₂ emissions relative to background is low. Remote sensing methods such as satellite imaging are capable of measuring total column integrated CO₂ on a global scale, but specific eruptions and volcanic plumes must be spatially and temporally targeted in order to capture events (Johnson et al., 2020). Atmospheric levels of CO₂ prevent accurate satellite imaging and remote laser methods require bulky equipment and have unrealistic line-of-site requirements.

¹Located in Jemez Springs, NM, United States.

OPEN ACCESS

Edited by:

Jonghoek Kim,
Hongik University, South Korea

Reviewed by:

Chunyan Zhang,
Nankai University, China
Ran Dai,
Purdue University, United States
David M. Pyle,
University of Oxford, United Kingdom

*Correspondence:

John Ericksen
johncarl@unm.edu

Specialty section:

This article was submitted to
Networked Control,
a section of the journal
Frontiers in Control Engineering

Received: 15 December 2021

Accepted: 31 January 2022

Published: 15 March 2022

Citation:

Ericksen J, Fricke GM, Nowicki S,
Fischer TP, Hayes JC, Rosenberger K,
Wolf SR, Fierro R and Moses ME
(2022) Aerial Survey Robotics in
Extreme Environments: Mapping
Volcanic CO₂ Emissions With
Flocking UAVs.
Front. Control. Eng. 3:836720.
doi: 10.3389/fcteg.2022.836720

But, relatively small instruments exist that can make very accurate point-measurements of CO₂. This requires that the measurement instrument be moved through the area of interest. In the case of volcanic emissions, this has been done by hand-carrying the instruments into dangerous locations or by human-piloted aircraft flying through hazardous volcanic plumes. Ground surveys, in addition to the risk involved, are biased by surveyors' inability to survey areas of unstable rock, sheer cliffs, scalding mud-pots, or (without specialized breathing equipment) areas with poisonous gas.

Several groups recently used remote-piloted aircraft to measure volcanic CO₂ at Manam volcano (Liu et al., 2020). That work provided new insights into volcanic CO₂ emissions but was hampered by the challenges of remote-piloting from great distances, with limited visibility, and under extremely hazardous conditions. Only a small subset of the drones deployed by the various teams involved was able to reach Manam volcano's plume, and only one drone survived the expedition.

Here we present the *first autonomous* surveys of volcanic CO₂. Autonomous UAVs are not restricted by line-of-sight or radio communication limitations, are not subject to hazardous ground conditions, and are immune to most poisonous gases. Autonomous UAVs can therefore survey volcanic CO₂ more effectively than human-piloted drones or ground-based surveys. Additionally, autonomous drones can coordinate their flight and sensor readings and make decisions based on those readings in real-time. Autonomy allows a team of UAVs, each equipped with a point-source measurement device, to become a much larger physically disconnected and therefore re-configurable sensor. In our case, three UAVs are required to map the CO₂ gradient fields required to localize CO₂ sources.

We designed, built, and field-tested a small swarm of UAVs called the Volcano Co-robot with Adaptive Natural algorithms (VolCAN) swarm. The VolCAN swarm executes a variety of surveillance algorithms to estimate the gas concentrations critical to volcanic eruption forecasting. The VolCAN swarm also implements a flocking algorithm for gradient descent to navigate to the locations where CO₂ is emitted from the ground. We test the swarm in simulation, in a hybrid field-simulation experiment in an open field, and ultimately perform multi-UAV atmospheric CO₂ emission surveys at the Valles Caldera supervolcano in New Mexico.

Volcanic Emissions

Worldwide, there are over 50 volcanic eruptions each year. More than 500 volcanoes are thought to be atmospheric CO₂ sources, yet less than 5% of those volcanoes have been surveyed (Fischer et al., 2019). Changes in the ratio of CO₂ to SO₂ from gas-emitting fumaroles have been observed to precede explosive volcanic eruptions (Aiuppa et al., 2010; Stix and de Moor, 2018), highlighting the potential of real-time gas measurements for eruption forecasting. Better forecasting of these eruptions is one of the three Grand Challenges recently highlighted by the National Academies because forecasting eruptions can save lives and mitigate volcanic hazards (Manga et al., 2017). Though dwarfed by anthropogenic emissions, volcanic CO₂ flux is also



FIGURE 1 | Flocking Dragonfly UAVs in formation. The flocking Dragonfly UAVs are used to survey volcanic CO₂ plumes.

important to a complete understanding of global volatile budget. (Fischer and Aiuppa, 2020).

Volcano surveys are hampered by the difficulty and danger of sampling gases in and around active craters. Volcanic CO₂ emissions can only be measured remotely by satellite when a satellite orbit is capable of capturing a specific location during an event. The NASA Orbital Climate Observatory has a 16-day repeat cycle and a narrow sampling width (Crisp et al., 2017), making targeting specific eruptions challenging. Ground-based remote sensing involves bulky instruments which are costly and difficult to deploy in remote areas (Aiuppa et al., 2015). Volcanologists, therefore, use hand-held detectors to gather point-source measurements by collecting and analyzing CO₂ concentration *in-situ* (Diaz et al., 2010). This is currently accomplished either by aircraft or by ground surveys (Chiodini et al., 1998), both of which are hazardous and inefficient. Our driving mission is to remove the human from these dangerous conditions while giving Volcanologists this critical data promptly.

Environmental Sensing by UAVs

We designed and built the Dragonfly UAV as shown in **Figure 1** as the VolCAN swarm hardware platform. The Dragonfly is designed to meet the requirements to survey active volcanoes in real-world conditions. These requirements are informed by our experiences surveying volcanoes with manually piloted UAVs (Liu et al., 2020). Currently, the state-of-the-art for volcanic UAV surveys is manually piloted using a single, typically combustion-powered, UAVs (James et al., 2020). Combustion engines introduce organic CO₂ into measurements which can be a source of significant error (Fischer and Lopez, 2016). Piloted flights introduce the possibility of human error and does not leverage the collected data in real-time. Our objective is to autonomously fly multiple UAVs to map CO₂ gas concentrations automatically and act as a single collaborative instrument capable of measuring multiple CO₂ reading point-sources at a time. This technique provides redundancy in gas readings, and the ability to calculate a gas concentration gradient. This follows our previous work where we developed and analyzed

the Loss-tolerant Cohesive UAV Swarm (LoCUS) Ericksen et al. (2020) algorithm.

Our work adds to the rapidly growing literature of environmental chemical sensing with small UAVs outlined by Burgués and Marco (2020), spurred by decreasing costs of chemical sensors and commercially-available drones. For a motion planning approach using chemical-sensing drones see Bourne et al. (2020). Nano drone chemical-sensing approaches have been demonstrated (Burgués et al., 2019; Anderson et al., 2020). However short flight times make them impractical for the larger-scale volcano surveys we target. Our Gradient following technique is similar to one demonstrated by Adamek et al. (2015) in aquatic environments for collaboratively mapping a lake boundary using three aquatic drones.

Autonomous robotic systems are becoming more resilient and capable of performing monitoring tasks in degraded and hazardous environments Chung et al. (2018). Applications include volcano monitoring Wood et al. (2020), subterranean exploration Dang et al. (2020), mapping mines Weber (1995), and nuclear facilities Thakur et al. (2020), surveying penguin colonies Shah et al. (2020), and disaster relief operations Sun et al. (2020), to name just a few. The underlying requirement across all these examples is one we share; to take the human out of harm's way, putting the risk on the expendable robotic hardware.

UAVs are an attractive solution for performing *in-situ* volcanic gas measurements. The Deep Carbon Observatory expedition to volcanoes in Papua New Guinea tested several remotely piloted, single-drone approaches to measuring gas plumes Liu et al. (2020). Several remote-piloted platforms were also tested at Masaya Volcano, Nicaragua Stix et al. (2018). Diaz et al. (2015) used UAVs equipped with miniature mass spectrometers to perform *in-situ* gas measurements the Turrialba Volcano in Costa Rica. The 2018 eruption at Kilauea Neal et al. (2019) and subsequent caldera collapse was extensively monitored with UAV-based imagery. These examples highlight hand-piloted UAVs and further underscore the need for automation in this space.

Vásárhelyi et al. (2014), developed and demonstrated a decentralized autonomous multi-drone flocking algorithm that avoids collisions between drones while maintaining a cohesive flock, a specialization of the canonical Boids flocking simulation in Reynolds (1987). We apply the collision-avoidance and velocity-matching techniques described there and add our formation strategy.

The contributions of this work are as follows:

1. We develop the Dragonfly UAV platform as a versatile autonomous volcano survey tool.
2. We implement rasterization survey algorithms and extend our LoCUS algorithm to use a flocking strategy to follow gas gradients to their source.
3. We demonstrate that the hardware platform and algorithms successfully measure known simulated gas concentrations and sources in the field using hybrid simulation/hardware experiments.
4. We validate that the VolCAN swarm can detect gas emissions and locate known gas sources in the challenging field

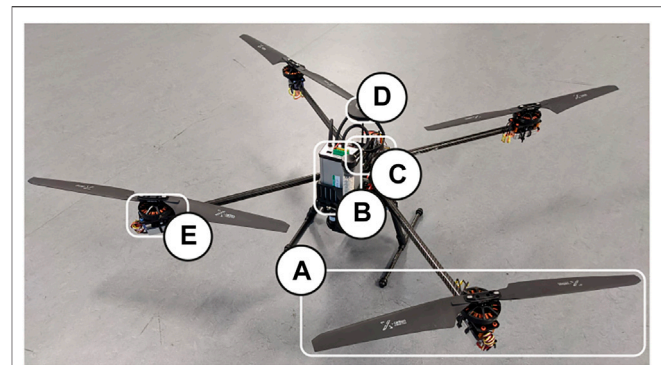


FIGURE 2 | Dragonfly UAV designed for volcano monitoring with arms and landing gear unfolded in flight-ready configuration. **(A)** 57 cm diameter propellers (highlighted for scale reference). **(B)** PP-Systems SBA-5 CO₂ sensor with absorber column weighing 0.5 kg. **(C)** Onboard flight computers and electronics, including a Raspberry Pi. **(D)** Hex Here2 GPS. **(E)** T-Motor MN6007 320 kV motors and Flame 60 A ESCs.

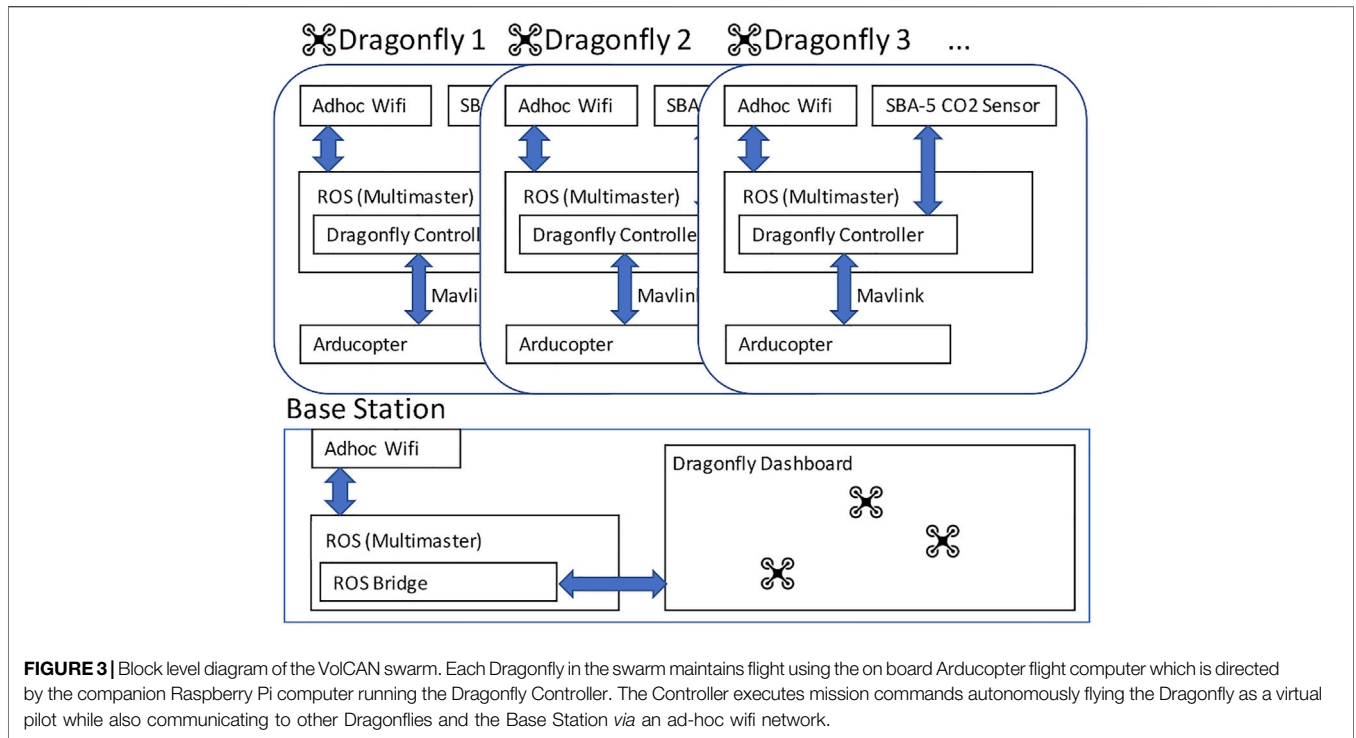
conditions at the Valles Caldera active volcano. Our field tests demonstrate the utility of distributed sensing and communication among coordinated UAVs for surveys in challenging environments.

2 METHODS

This section describes the development of the VolCAN swarm hardware and software as well as testing in simulation, hybrid simulation/field experiments, and natural field conditions. Simulation experiments were performed using the Gazebo real-physics simulator (Koenig and Howard, 2004). Field experiments were conducted at two New Mexico, US sites: Balloon Fiesta Park in Albuquerque and near the Valles Caldera supervolcano.

2.1 Dragonfly Design and Mission Parameters

We designed and built the Dragonfly UAV (Figure 2) to fly with a 2 kg payload, including a CO₂ sensor, for 1 h duration. We chose larger motors and propellers to provide enough thrust to be able to fly in high winds. The highest wind speed under which we successfully tested the platform was 16 m/s. During hover and under normal flight dynamics, the system uses between 15 and 20 A. The Dragonfly folds to fit in a backpack case for transportation on foot to volcanic field sites. The foldable Tarot 650 frame allows for a variety of sensor configurations and payloads mounted to the payload rails. The UAVs communicate with each other and a base station through an ad-hoc wifi network. They can operate autonomously and under the guidance of a *scientist-in-the-loop* (Aodha et al., 2014). The Dragonfly design is centered around the MavROS programming interface to implement autonomous control. The Dragonflies were built using commodity hardware and 3D-printed parts to reduce costs and make it possible to do common repairs on-site.



The laboratory-grade PP-Systems SBA-5 CO₂ detection sensor was chosen to fill the requirement of CO₂ gas concentration sensing because its durability, accuracy of 1–2 ppm, wide detection range, and mass of only 200 g (Stix et al., 2018). The sensor is also capable of operating at high altitudes and in a wide range of operating temperatures (Lee et al., 2016; Ilanko et al., 2019). In our initial design experiments rotor wash was a confounding factor in CO₂ measurement, for scales less than 3 m; however, 3 m is below the relevant resolution for volcanic plumes.

2.2 The Dragonfly Software Platform

Dragonfly software is comprised of two main components: the Dragonfly dashboard and the onboard controller. These components integrate the ecosystem of modules to control the VolCAN swarm as a whole as depicted in **Figure 3**.

The Dragonfly dashboard² is a human-friendly interface for planning missions. The dashboard provides a convenient Graphical User Interface (GUI) ground station for visualizing and managing the swarm of networked Dragonflies on a 3D map. The dashboard gives the user the ability to control and provide expert feedback to the entire swarm, a foundation of the scientist-in-the-loop goal.

The Dragonfly Controller³ acts as a virtual pilot. It is a collection of Robot Operating System (ROS) Quigley et al.

(2009) melodic nodes running on the onboard companion computer. These nodes were run in a multimaster ROS environment, allowing ROS to broker communication between Dragonflies and the ground station.

The Dragonfly Controller contains the following ROS nodes.

1. CO₂ ROS Sensor Node publishes data from the connected SBA-5 CO₂ sensor at 10 Hz. This allows any Dragonfly to stream any other Dragonfly’s CO₂ readings.
2. Data Logger records CO₂ measurements and their global positioning system (GPS) coordinates.
3. Command Service provides high-level flight commands to operate the Dragonflies, including common actions like *takeoff*, *land*, *return to launch (RTL)*, *goto waypoint* along with the following actions:
 - a. Execute *DDSA* or *Lawnmower* (**Section 2.3**).
 - b. *Flock* and *Coordinated Gradient Descent*. These two commands direct the Dragonflies to organize into a flock and follow CO₂ gradients (**Section 2.4**).
 - c. *Mission* executes a list of actions in series on the Dragonflies but in parallel across the swarm. Mission actions included all of the command service actions along with a *semaphore* that acts as an execution barrier to synchronize survey algorithm execution across multiple Dragonflies.

2.3 Preplanned Survey Algorithms

To map the CO₂ of a region of interest, we implement two rasterization survey algorithms: the lawnmower survey algorithm and the distributed deterministic spiral search algorithm (DDSA) (Fricke et al., 2016; Aggarwal et al., 2019) survey algorithm. Both

²Dragonfly Dashboard source code: <https://github.com/BCLab-UNM/dragonfly-dashboard/tree/FRONTIERS2021>.

³Dragonfly Controller source code: <https://github.com/BCLab-UNM/dragonfly-controller/tree/FRONTIERS2021>.

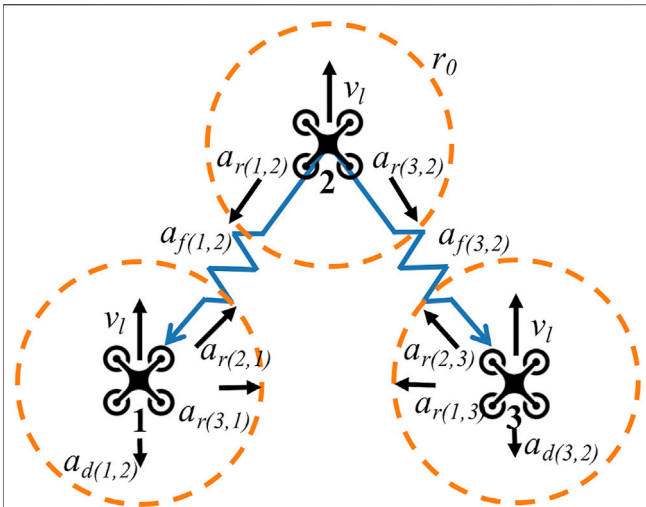


FIGURE 4 | Flocking Algorithm. This diagram highlights the constituent forces acting on each Dragonfly, which are summed to produce the v_i control velocity on each of the three drones flocking formation. The dotted circles represent the minimum repulsion radius r_0 where $a_{r(i,j)}$ pushes two drones apart (see Eq. 1). The springs labeled with $a_{f(i,\ell)}$ are the flocking forces maintaining the drone formation in relation to Dragonfly 2 (see Eq. 2). $a_{d(i,\ell)}$ is the velocity dampening force (see Eq. 3), and v_ℓ is the leader velocity applied to the flock (see Eq. 4).

of these algorithms create an exhaustive 2D rasterization map by visiting each area within a given radius. The lawnmower algorithm scans a polygon region by incrementally following longitudinal passes across a predefined region. We implement the lawnmower algorithm using a linear programming framework to perform boundary calculations against a user-defined polygon. This technique allows the mapping of irregularly shaped regions and avoids hazards such as trees, power lines, and sudden elevation changes which are commonplace in the target environments. The DDSA algorithm is a multi-agent spiral search algorithm that navigates multiple drones in interleaved square spiral paths. Unlike the lawnmower algorithm, the DDSA algorithm guarantees collision avoidance because the interleaved paths never cross. The output of these algorithms are waypoints which the Dragonfly autonomously navigates during a mission. GPS stamped CO₂ data sets logged from these flights are ideal to create Kriging CO₂ concentration maps due to their uniform region coverage.

2.4 Flocking Algorithm for Gradient Descent

While the lawnmower survey algorithm is an autonomous pre-planned algorithm, the gradient descent flocking algorithm adapts the paths of the UAVs in response to the data they sense and communicate to each other. The gradient descent algorithm goal is for the Dragonflies to navigate to an unmapped location where the gas flux is highest which would identify the location from which the gas is emitted without spending the extra time to rasterize the surrounding area. This increase in efficiency follows work by Aggarwal et al. (2019). To spatially coordinate multiple Dragonflies, we used a leader-based flocking algorithm following Vásárhelyi et al. (2014) detailed in Figure 4.

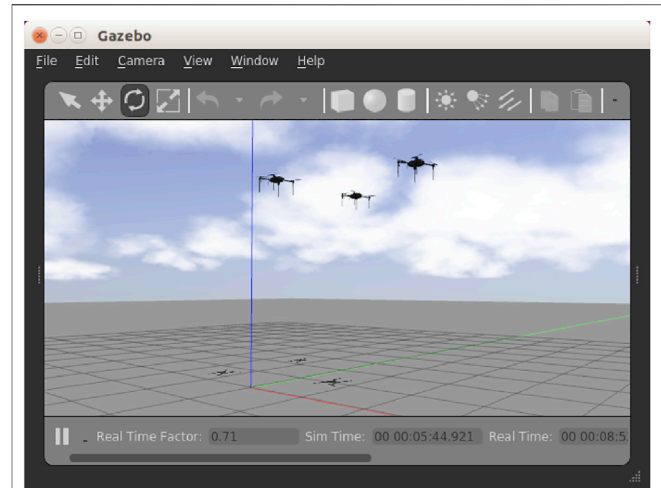


FIGURE 5 | Algorithm Testing in Simulation with three simulated Dragonflies, each running their own instance of Arducopter and the Dragonfly Controller.

Flocking drones avoid collisions by using a drone i , to drone j , repulsion force a_r . This force acts like a virtual spring between drones within a radius r_0 of each other. r_1 acts as a maximum repulsion force:

$$a_r = - \sum_{\forall i,j: i \neq j, |x_{i,j}| \leq r_0} \min(r_1, r_0 - |x_{i,j}|) \frac{x_{i,j}}{|x_{i,j}|} \tag{1}$$

To maintain the formation, a potential well applies force $a_{f(i,\ell)}$, aligns each dragonfly at their respective positions $x_{f(i)}$. $x_{f(i)}$ is a specified offset from the leader ℓ of $x_{\ell,i}$ given by,

$$a_{f(i,\ell)} = \frac{x_{\ell,i} - x_{f(i)}}{|x_{\ell,i} - x_{f(i)}|} \tag{2}$$

A dampening term is used to prevent overshooting the leader ℓ when matching velocities:

$$a_{d(i,\ell)} = v_\ell - v_i \tag{3}$$

To achieve formation flocking each force vector is scaled by a corresponding gain term c , c_f , and c_d and update time Δt to give a velocity vector v_i m/s:

$$v_i = v_\ell + \Delta t (c_r a_r + c_f a_{f(i,\ell)} + c_d a_{d(i,\ell)}) \tag{4}$$

Formation flocking is implemented in Algorithm 1. FLOCK is called on an interval, once per Δt time-step which updates the velocity of the given drone in the flock by calling the SETVELOCITY function.

In previous work, we developed the LoCUS algorithm for formation flying which used a lock-step technique to move the formation in space (Ericksen et al., 2020). We replaced this technique in LoCUS with the above flocking algorithm. This enabled the inherent dynamism of flocks to make collision avoidance more natural and, in general, made the group of UAVs more responsive to changing inputs.

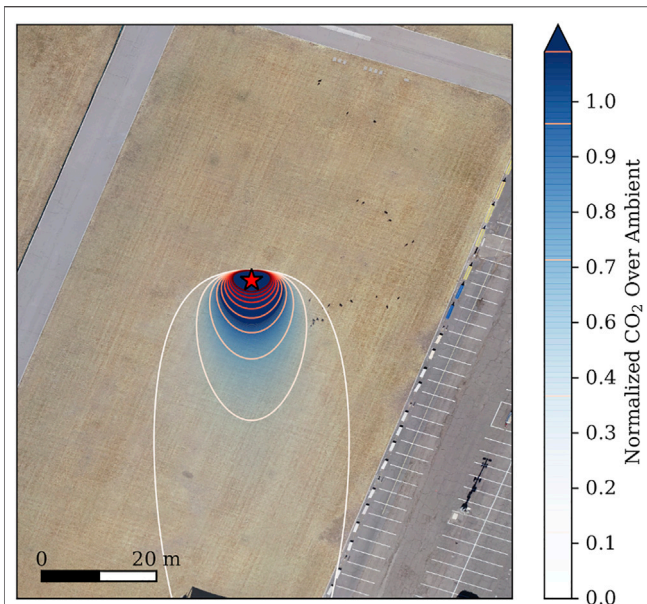


FIGURE 6 | Virtual Plume Plotted on Balloon Fiesta Park. The Virtual Plume, with the source specified to be the middle of the field, is configured with a northerly wind producing the long tail. The isoconcentration lines are added to accentuate the plume’s shape at lower concentration levels.

Algorithm 1. Flocking Velocity Update Algorithm.

```

function FLOCK(leaderIndex, selfIndex, positions, velocities)
  ar ← REPULSION(selfIndex, positions)
  af ← FORMATION(leaderIndex, selfIndex, positions)
  ad ← velocities[leaderIndex] - velocities[selfIndex]
  v ← velocities[leaderIndex] + Δt(crar + cfaf + cdad)
  SETVELOCITY(v)
end function
    
```

The dragonfly flock performs gradient descent by following the plume’s atmospheric dispersion gradient towards the concentration maximum at the source of the plume. The gradient is calculated by the lead drone by aggregating CO₂ measurement point-sources φ and corresponding 2D spatial positions (x, y) of each agent α in the swarm at each time step. This data is fit with a linear slope b relating point-source concentration to position in the form $Ab + \epsilon = s$, and the slope parameter b is calculated by minimizing the magnitude of the error term ϵ through least-squares approximation:

$$\underbrace{\begin{bmatrix} 1 & \alpha[1].x & \alpha[1].y \\ 1 & \alpha[2].x & \alpha[2].y \\ \vdots & \vdots & \vdots \end{bmatrix}}_A \underbrace{\begin{bmatrix} b[0] \\ b[1] \\ b[2] \end{bmatrix}}_b + \underbrace{\begin{bmatrix} \epsilon[0] \\ \epsilon[1] \\ \vdots \end{bmatrix}}_\epsilon = \underbrace{\begin{bmatrix} \alpha[1].\varphi \\ \alpha[2].\varphi \\ \vdots \end{bmatrix}}_s \quad (5)$$

The linear fit slope b components include the vector $(b[1], b[2])$ which points in the direction of maximum CO₂. To gradient descend in two dimensions, at least three drones are required for the linear fit. Additional drones above this minimum provide redundancy and an averaging effect across the swarm’s CO₂ readings.

2.5 Simulation

To facilitate repeatable experiments under controlled conditions and to accelerate development, the Dragonfly hardware,

Ardupilot flight control software, and the onboard Dragonfly Controller were implemented in the Gazebo real-physics simulation as shown in Figure 5.⁴ We ran the same software in simulation (also known as Simulation-in-the-Loop) as in the physical hardware which expedited algorithm prototyping and debugging before flying in a physical UAVs.

We define a Virtual Plume for use in Gazebo simulations and hardware/simulation hybrid experiments (described in the next section). The plume model is a horizontal 2D slice through a 3D Gaussian plume. The concentration is calculated from a x, y GPS coordinate offset with constants stack height H , wind speed u , emission rate Q , and diffusion rate K (Stockie, 2011):

$$PLUME(x, y) = \frac{Q}{2\pi Kx} \exp\left(-\frac{u(y^2 + H^2)}{4 Kx}\right). \quad (6)$$

3 RESULTS

Experiments were conducted at two field sites. First, hardware Dragonflies were flown in an open field and tasked with the mission of mapping and finding the source of a virtual plume. This allowed us to evaluate how the algorithms would behave in real hardware in an outdoor environment. The virtual plume allowed us to evaluate how effectively the UAVs would map known gas concentrations and the known source location of the simulated CO₂ plume.

Second, experiments were performed at a natural volcanic site to test the plume-sensing capabilities of the Dragonfly platform under real-world conditions. Previous field studies were conducted by geoscientists at the site and sites of elevated CO₂ were identified in Golla (2019). This provided us with a likely location for CO₂ emissions; however, CO₂ emissions change frequently, and measurements are affected by wind and temperature. Thus, it is difficult to acquire accurate ground truth. Therefore, we used the simulated plume at the first field site to show the VolCAN swarm could accurately map CO₂ concentrations and source location. The field study at Valles Caldera volcano demonstrated that the swarm could produce rasterized surveys and flock to a suspected source of CO₂ under difficult field conditions but where there is uncertainty in true sources and concentrations of CO₂. All field experiments were conducted according to US Federal Aviation Administration (FAA) Unmanned Aircraft Systems (UAS) regulations and with permission in relevant airspaces.

3.1 Open Field Experiments

Our open field site was the large flying field of Balloon Fiesta Park in Albuquerque, New Mexico. We used the Virtual Plume during field experiments to add a plume for the algorithms to map and follow. We centered the Virtual Plume at latitude 35.19465,

⁴Simulation source code: <https://github.com/BCLab-UNM/dragonfly-sim/tree/FRONTIERS2021>.

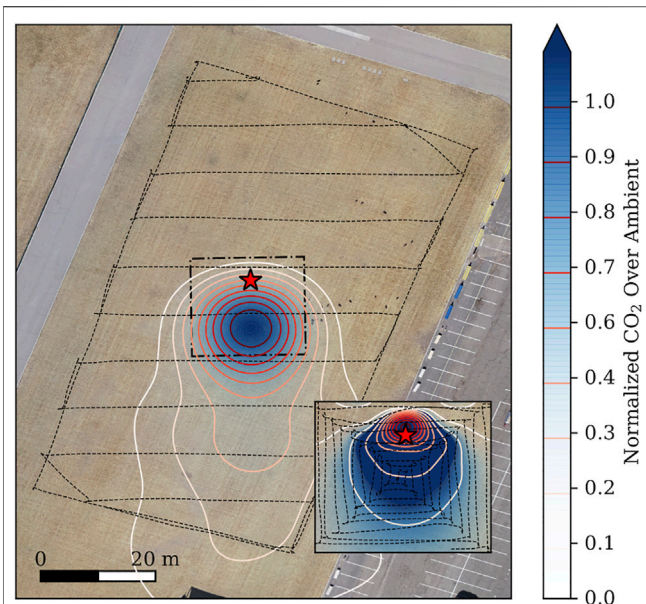


FIGURE 7 | Coarse-grained lawn timer flight and more thorough survey using the DDSA (inset) flight at Balloon Fiesta Park. Each lawn timer pass across the field is separated by 10 m whereas each arm of the DDSA is separated by 1 m. Virtual plume data collected on the field is represented in the Kriging map. This map is compared with the Virtual Plume plot to see how the Kriging map represents the plume with limited information.

longitude -106.59625 with parameters $H = 2$ m, $u = 1$ m/s, $Q = 5$ kg/s, $K = 2$ kg/s.

3.1.1 Rasterization Survey

To map the virtual plume a large-scale 10 m resolution rasterization survey of the field was performed using the lawn timer algorithm within a polygon outlining the designated field. The Dragonfly flew at 10 m altitude, with each longitudinal pass at 10 m spacing. We used the lawn timer survey to produce a Kriging heat map of the virtual plume seen in **Figure 6**.

For a fine-grained 1 m resolution survey of the virtual plume, we executed a DDSA slightly to the north of the detected plume. We used a single Dragonfly in the DDSA with spiral arms separated by 1 m spacing, and we performed 10 loops at a single altitude of 10 m. The goal was to produce a detailed Kriging heat map of the Virtual Plume.

We generated two maps to test the ability of the two sample rasterization methods to recreate the simulated plume over the open field. The ground-truth virtual plume is depicted in **Figure 6**. The coarse-grained map of CO₂ generated from data using the lawn timer algorithm and the fine-grained map generated using the DDSA are displayed in **Figure 7**. The CO₂ plume is visible in the center of the field, even with the limited data available from the 10 m separated longitudinal passes of the lawn timer algorithm. The DDSA map, displayed in the lower right detail, has more structure due to the finer-grained arm separation of 1 m that closely resembles the simulated plume. The fine-grained DDSA algorithm estimated the highest CO₂

concentration very close to the location of the plume source (indicated by the red star). To compare the sampled maps S against the ground-truth maps G of shared dimensions (m, n) , we find the mean absolute difference MD over the 2D space of these normalized data sets:

$$MD(S, G) = \frac{\sum_{i,j} |S_{i,j} - G_{i,j}|}{m \times n} \quad (7)$$

The coarse-grained course-grained¹ lawn timer mean absolute difference is 0.1306 and the fine-grained DDSA mean absolute difference is 0.0380 indicating the higher resolution of the fine-grained DDSA was able to reproduce a more accurate representation of the ground-truth data. In addition, the course-grained lawn timer estimated the source at approximately 10 m away from its actual location whereas the fine-grained DDSA estimated the source at approximately 1 m from the ground-truth source, again representing that a finer-grained map produces a more accurate representation of the ground truth.

3.1.2 Flocking and Gradient Descent

We implemented LoCUS on three Dragonflies with Dragonfly 2 as the lead UAV and Dragonfly 1 and three oriented at (x, y) offsets $(-6$ m, -6 m) and $(6$ m, -6 m), respectively. This produced a V-formation orienting Dragonfly 1 and three orthogonally *via* Dragonfly 2, which is ideal for detecting a 2D gradient and separating the drones to avoid collisions due to GPS accuracy. For these experiments, we flew each Dragonfly at different altitudes, separated by 1 m, as an additional safety measure to avoid mid-air collisions. To test gradient descent, Dragonfly 2 was commanded to perform gradient descent autonomous flight using CO₂ readings correlated with location information from Dragonfly 1, 2, and 3. The Dragonfly flock was positioned in the

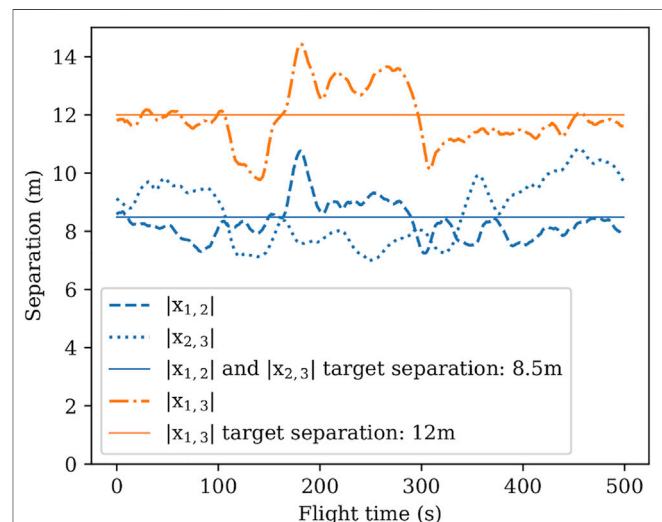


FIGURE 8 | Flocking Algorithm Achieves Target Separation. The distance magnitude between Dragonfly a and b is signified $|x_{a,b}|$. All three Dragonflies stay well away from each other, only reaching a minimum distance of 7.0 m. Likewise, Dragonflies 1 and 2 stay within a maximum of 11 m of Dragonfly 2, keeping the flock in formation.

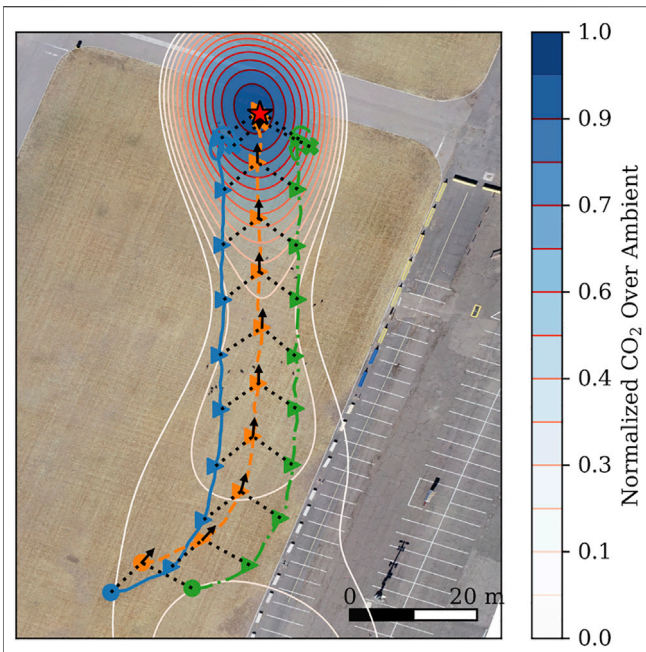


FIGURE 9 | Flocking Gradient Descent in the Field mapping a virtual plume. Colored lines represent the flight paths of the Dragonfly flock in V-formation following the gradient. Dotted lines between key points in time, marked as directional triangles, indicate the network connections during flight. Arrows indicate the normalized gradient of the virtual plume, which is represented as a Kriging heat map. From the starting point, the flight path length was about 100 m and took the flock about 2 min to reach and identify the plume’s maximum concentration, which is within 0.30 m of the source. The Virtual Plume was moved up field from the previous experiments to allow for more travel distance of the flock.

plume’s tail to start with an initial signal that was used to follow the virtual CO₂ plume towards the source. The goal of this experiment was for the flock to identify the source of the plume represented by the location with maximum CO₂ concentration.

The purpose of flocking is to identify the location with the highest CO₂ concentration using multiple UAVs close while preventing collisions. **Figure 8** shows the Euclidean distances between drones during a manually piloted test flight. Dragonfly 1 and three reach a minimum and maximum distance between themselves and the lead Dragonfly 2 of 7.0 and 11 m, respectively. These distances lie within 2.3 m of the ideal configured distance of 8.5 m. Similarly, Dragonfly 1 and three stay within 2.4 m of the ideal configured distance of 12 m. All three Dragonflies fly more than 6 m away from each other, greater than the acceptable GPS error radius of 6 m. This effectively kept each drone in an orthogonal orientation which is essential for collecting a 2D sample gradient vector while avoiding collisions between members of the flock.

Figure 9 shows the path of the three flocking Dragonflies as they follow the gradient vector indicated by the black arrow. The arrow is a normalized representation of the $(b [1], b [2])$ vector described in **Section 2.4**. Dragonfly 2 successfully navigates into the virtual CO₂ plume by following the b vector, finding the

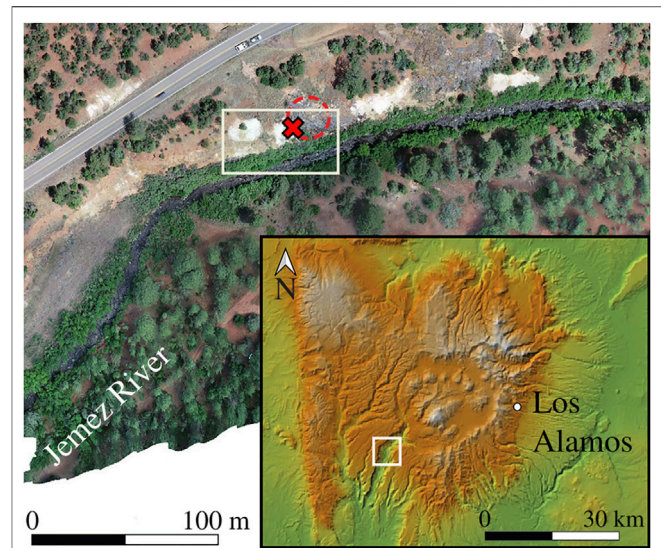
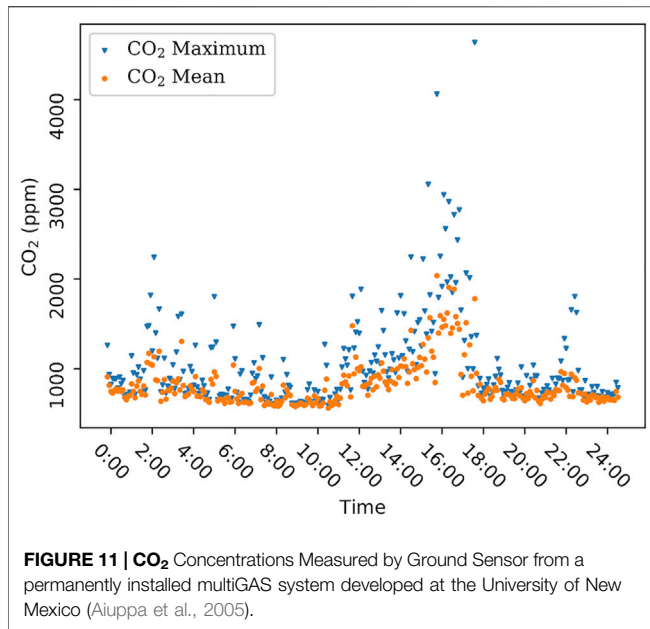


FIGURE 10 | Valles Caldera Supervolcano: Overview of Field Site. A visible imagery mosaic of the field site, with an inset displaying the terrain of the Valles Caldera volcano. In previous surveys, CO₂ emissions were associated with the white calcite surface deposits (Fahilly, 2020). The calcite associate with the primary CO₂ source, circled in red, has been obscured by brush. The white rectangles indicates the survey site. The red x indicates the position of a fixed ground sensor.

maximum CO₂ value of 710 ppm. This result matches our results from Ericksen et al. (2020), where the flock can quickly and directly follow the plume’s gradient back to the source. Just as with the flocking result, we produce an accurate Kriging map from the data collected across all three drones, which produces a map similar to the one produced in **Figures 7, 9**.

3.2 Volcano Field Tests

Valles Caldera is a supervolcano in northern New Mexico (**Figure 10**). The caldera is more than 22 km in diameter with CO₂ emissions at several sites (Goff and Janik, 2002). The field site chosen for VolCAN swarm surveys and flocking is a small canyon formed by the Jemez River. CO₂ degases diffusely out of the ground on the northern side of the canyon (Golla, 2019). The location offers a challenging flight environment because of the forest and steep canyon hills on either side. This bracketed the available flight space and required extremely accurate mission planning and flight control. Our challenge was to balance flying low enough to detect the degassing CO₂ emitted from the ground, high enough to clear the tallest trees, and within a boundary to not collide with the canyon hills. There was quite a bit of effort put into mission plans including sighting the treetops, creating and analyzing a topology map, reviewing CO₂ data collected during the missions, and manually adjusting mission boundaries. Additionally, the design and tuning of the Dragonflies played a large component in flying accurately even in windy conditions. Despite our efforts, We experienced occasional catastrophic collisions with trees while tuning flight parameters. Unfortunately, damage to the platform significantly affects the flight characteristics of the UAVs which underscores the



importance of planning flights clear of obstacles. While Valles Caldera is safe for researchers because there is no current danger of eruption, it is an ideal real-world test site for the VolCAN swarm due to its active release of gasses and its topology typical of challenges in volcanic regions.

The site was previously surveyed in Rahilly (2020) for CO₂ emissions. The evidence for historical emissions is the white areas of hydrothermal alteration. A permanent ground sensor is located at the location of the highest CO₂ emissions indicated by the red star in **Figure 10**. An example of the CO₂ emissions detected from the ground sensor is shown in **Figure 11** and highlights the variability of CO₂ over time.

3.2.1 Rasterization Survey

We executed a large-scale rasterization of the area at 50 m above the canyon floor takeoff location. Flying at this height cleared the tallest trees in the area but still was able to detect a difference in CO₂. The large-scale rasterization lawnmower was executed with longitudinal passes at 5 m spacing. Additionally, we flew the lawnmower with three dragonflies in flocking v-formation with Dragonfly 1 and three oriented at (x, y) offsets $(-6\text{ m}, -6\text{ m})$ and $(6\text{ m}, -6\text{ m})$, respectively. Flocking allowed us to gather redundant data during the rasterization survey. By simultaneously collecting CO₂ data from multiple nearby UAVs, we increased the volume of data collected during the mission to create more detailed maps. Additionally, this approach allowed us to compare CO₂ concentrations from three different sensors to understand variation in both the environment and the sensors over the same period. CO₂ concentration readings from this survey were gathered and used to generate a Kriging map of the concentration gradient against aerial photography of the region.⁵

⁵Video of the survey: <https://youtu.be/VVz68ZqhD8k>.

Figure 12 shows the Kriging map generated from CO₂ data combined from all dragonflies in the flock. The Kriging map shows a complex distribution of CO₂ with the highest elevated CO₂ emanating from a previously unknown source to the east, and an elevated plume above and slightly to the east of the known source indicated by the dashed red circle. Detected CO₂ across the swarm and overtime is normalized to produce the percentage difference in CO₂ shown in the figure. Normalization is performed by linearly scaling the data to the minimum and maximum CO₂ reading over the data set. Detected CO₂ readings were between 410 and 430 ppm across Dragonfly 1, 2, and 3. The total flight time to rasterize the area was 13 min 42 s.

3.2.2 Flocking and Gradient Descent

We followed a CO₂ gradient to its source by performing gradient descent with the following mission. First, we flocked Dragonflies 1, 2, and three in V-formation with Dragonfly 2 as the leader. We then navigated the flock to a waypoint position south of the known source along the Jemez River. Finally, we triggered Dragonfly 2 to follow the gradient calculated from data collected from the swarm. The goal of this experiment is to validate that gradient descent can navigate the swarm of drones using a previously identified natural source of CO₂.

In addition to the Kriging map survey, **Figure 12** displays the path of the Dragonfly flock following the CO₂ concentration gradient using gradient descent in real-time. The path starts to the south of the known source and proceeds to move north until a maximum CO₂ of 430 ppm was reached due east of the known source indicated by the dashed red circle. This path follows the gradient previously detected by the rasterized survey and shows the flock effectively using the input CO₂ data to fly towards the known source plume's highest concentration. The total flight time for the gradient descent portion of the mission was 25 s.

4 DISCUSSION

Our results show that the Dragonfly UAV platform effectively maps aerial CO₂ emissions in the challenging, real-world conditions of volcanic environments. We developed the Dragonfly UAVs platform with the navigational capabilities, flight duration, and payload capacity foundations to be able to accurately collect CO₂ gasses, analyze them *in-situ*, and respond to the detected concentrations in real-time across multiple UAVs. This culminated in the rasterization survey of a known hot-spot in the Valles Caldera where we autonomously flew the VolCAN swarm in formation and mapped the CO₂ at 50 m. This highlighted the elevated CO₂ around the known source but also indicated an additional previously unknown source to the northeast. Additionally, we executed an autonomous gradient descent that successfully navigated into the elevated CO₂ near the known source in the area. These field tests demonstrate the utility of the VolCAN swarm in mapping and navigating CO₂ gradients in real-world extreme environments.

The development of the Dragonfly UAV platform took considerable effort to meet the mission requirements. The biggest driving requirement was the flight time which dictated

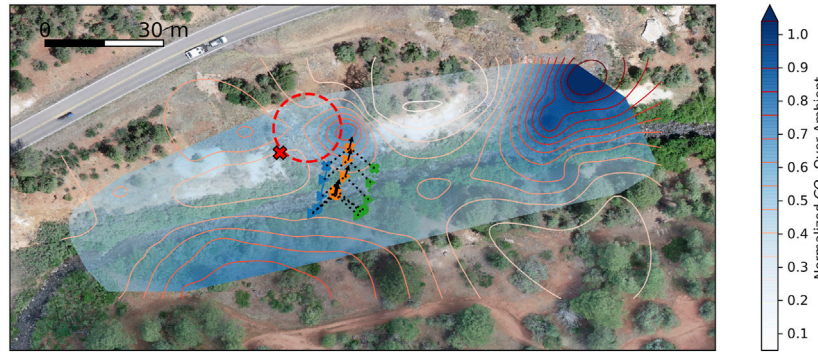


FIGURE 12 | Kriging isoconcentration map produced from CO₂ data collected during the flight. This map is the result of data collected using three Dragonfly drones flying the pattern in formation. Regions of note are the elevated concentration above and slightly to the east of the known source outlined in the dashed-red circle and the region in the east of the plot indicating another CO₂ source plume. The path of the flock of Dragonflies is drawn as they follow the detected gradient which corresponds to the known source and previously mapped gradient.

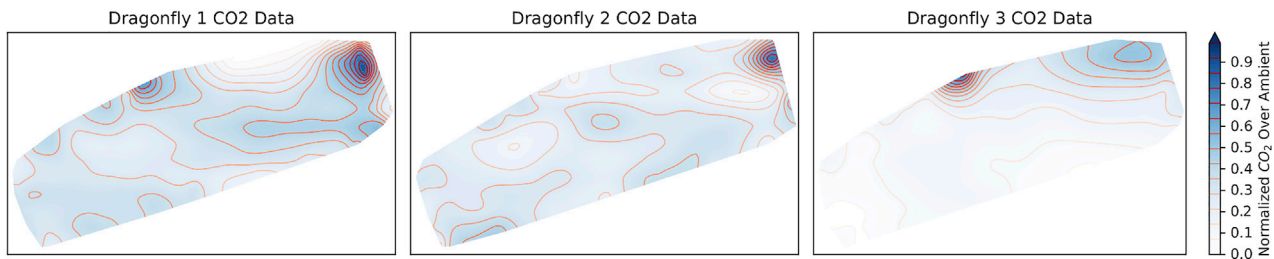


FIGURE 13 | Kriging maps of the individual component Dragonfly CO₂ readings combined in **Figure 12**. Of note are the common elevated regions in the upper right and mid-left of each survey. These common readings confirm that there is elevated CO₂ in that region of the sky.

the overall weight of the aircraft, specifically the large battery requirements. This drove motor and propeller sizes to be able to produce enough lift with agility. To control the aircraft, we found that the flight controller PID tune was critical and only found success after hand-tuning these parameters. Tuning the PID loop to be somewhat aggressive resulted in an aircraft that would behave well in gusty high wind conditions, perform as expected around other aircraft, and mirror the aircraft’s simulation behavior.

Trials of the Dragonfly UAV in the open field helped solidify the algorithms developed in simulation in a real-world environment. Flying in the semi-controlled environment with a virtual plume ensured that we could map a CO₂ plume and represent it with a level of confidence. Our results show that the coarse-grainedcourse-grained¹ rasterization produced a map with a mean absolute difference of 13% to ground truth, with a smaller mean absolute difference of 3% for the fine-grained rasterization. Flocking the Dragonflies and following the virtual plume gradient demonstrated that we could identify the source of the plume, represented by the highest CO₂ concentration in the gradient.

Mapping the known sources around the Jemez river in the Valles Caldera offered a chance to test the VolCAN swarm against real CO₂ sources. To map the overall region we had to fly at a high

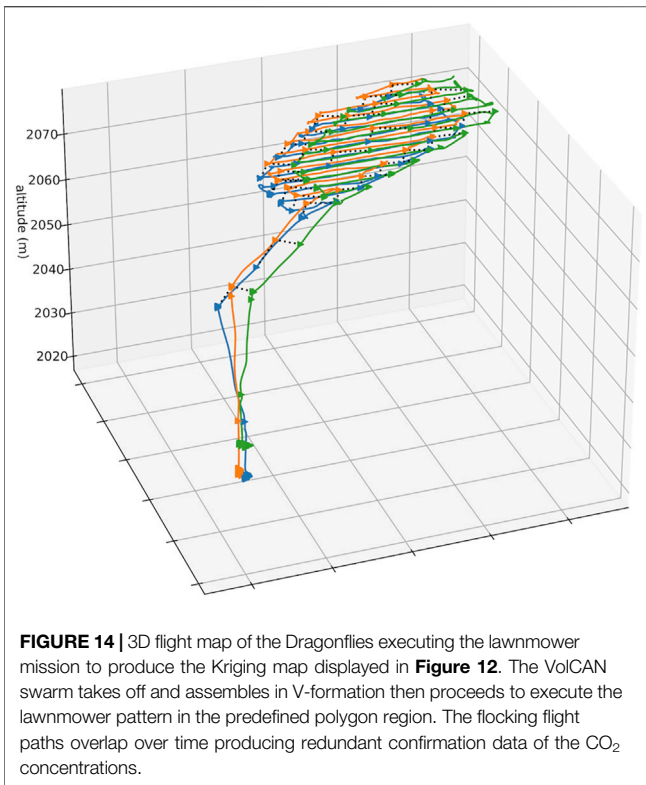
elevation above ground level to avoid the tree canopy obstructions. This resulted in a relatively low CO₂ signal compared with ground measurements. However, due to the accuracy of the SBA-5, we were still able to detect differences on the order of 1 ppm making the collection missions still effective. This further highlights the efficacy of our technique in mapping and responding to the aerial CO₂ signal.

The missions at the Valles Caldera highlighted the survey speeds. During the same day as the aerial surveys, a ground survey team was gathering CO₂ ground flux and concentration readings using portable CO₂ fluxmeters. Their survey of a region similar to the lawnmower survey took 8 h to complete. In comparison, the lawnmower survey took less than 15 min and the gradient descent took less than 30 s, each an order of magnitude faster than the previous.

Our survey methods are also applicable to a variety of other environmental monitoring tasks that require *in-situ* measurements and efficient localization, such as detecting gas line leaks and environmental monitoring.

4.1 Caveats and Future Work

With any data collection task, especially one of such a dynamic process, the challenge is to tie the data back to known ground truth. In our case, the data and Kriging maps demonstrate a high



correlation to the virtual plume in the open field environment. This ensures that data collection missions in the field represent a facsimile of what is truly occurring. That being said, the data represented by flying high above the ground and known sources in Jemez Springs should be interpreted with caution. The low CO₂ readings did correlate to the known source on the ground, and indicate another source to the northeast, but a slight breeze can easily shift the location of these gasses. We propose that mapping larger regions, on the order of 100 m will help in localizing gas sources or taking into account wind direction and speed to produce an offset.

Upon inspection of the data used for gradient descent, it is feasible that the low CO₂ concentrations and proximity of each drone to each other that differences in sensor temperatures and calibration played a factor in the detected gradient. The bottom line is that the drones did respond to the gradient and future work will be dedicated to determining the spacing of the flock to best gather and follow gradients.

With the development of the VolCAN swarm including the Dragonfly platform and the algorithms to map and follow

gradients, the next step is to further automate the swarm's behavior. This includes handing over decisions when and where to perform a survey and at what resolution, where to perform gradient descent to find the source of emissions, and utilizing battery life to maximize the investigation of a region. Also, automating the initial setup and mission parameters like the elevation to clear obstacles, and the overall flight boundaries would help speed the overall mission.

DATA AVAILABILITY STATEMENT

The original contributions presented in the study are included in the article/Supplementary Material, further inquiries can be directed to the corresponding author.

AUTHOR CONTRIBUTIONS

JE is the corresponding author and main contributor to the publication. GF served as the second seat, all supported by RF and MM. SN and TF provided support from Earth and Planetary Sciences perspective. JH, KR, and SW provided support on expeditions, processing data, and editing the manuscript.

FUNDING

JE support provided by Department of Energy's Kansas City National Security Campus, operated by Honeywell Federal Manufacturing and Technologies, LLC under contract number DE-NA0002839. GF, SN, TF, RF, and MM support provided by the VolCAN project under National Science Foundation grant 2024520. Support was also provided by a Google CSR award. This study received funding from Google and Honeywell Federal Manufacturing and Technologies, LLC. The funder was not involved in the study design, collection, analysis, interpretation of data, the writing of this article or the decision to submit it for publication. All authors declare no other competing interests.

ACKNOWLEDGMENTS

We thank the Hummingbird Music Camp and the City of Albuquerque Parks and Recreation for their support. We thank Jarett Jones and Brian Verkaart for technical advice supporting the development of the Dragonflies.

REFERENCES

- Adamek, T., Kitts, C. A., and Mas, I. (2015). Gradient-Based Cluster Space Navigation for Autonomous Surface Vessels. *Ieee/asme Trans. Mechatron.* 20, 506–518. doi:10.1109/TMECH.2013.2297152
- Aggarwal, A., Gupta, D., Vining, W. F., Fricke, G. M., and Moses, M. E. (2019). "Ignorance is Not Bliss: An Analysis of Central-Place Foraging Algorithms," in *2019 IEEE/RSJ International Conference on Intelligent Robots and Systems (IROS)* (IEEE), 6510–6517.
- Aiuppa, A., Fiorani, L., Santoro, S., Parracino, S., Nuvoli, M., Chiodini, G., et al. (2015). New Ground-Based Lidar Enables Volcanic CO₂ Flux Measurements. *Sci. Rep.* 5, 13614–13712. doi:10.1038/srep13614
- Aiuppa, A., Burton, M., Caltabiano, T., Giudice, G., Guerrieri, S., Liuzzo, M., et al. (2010). Unusually Large Magmatic CO₂gas Emissions Prior to a Basaltic Paroxysm. *Geophys. Res. Lett.* 37, a–n. doi:10.1029/2010GL043837

- Aiuppa, A., Federico, C., Giudice, G., and Gurrieri, S. (2005). Chemical mapping of a fumarolic field: la fossa crater, vulcano island (aeolian islands, italy). *Geophys. Res. Lett.* 32, 1023207. doi:10.1029/2005gl023207
- Anderson, M. J., Sullivan, J. G., Horiuchi, T. K., Fuller, S. B., and Daniel, T. L. (2020). A Bio-Hybrid Odor-Guided Autonomous palm-sized Air Vehicle. *Bioinspir. Biomim.* 16, 026002. doi:10.1088/1748-3190/abb8d1
- Aodha, O. M., Stathopoulos, V., Brostow, G. J., Terry, M., Girolami, M., and Jones, K. E. (2014). "Putting the Scientist in the Loop -- Accelerating Scientific Progress with Interactive Machine Learning," in Proceedings - International Conference on Pattern Recognition, Stockholm, Sweden, 24-28 Aug. 2014 (IEEE). doi:10.1109/ICPR.2014.12
- Bourne, J. R., Goodell, M. N., He, X., Steiner, J. A., and Leang, K. K. (2020). Decentralized Multi-Agent Information-Theoretic Control for Target Estimation and Localization: Finding Gas Leaks. *Int. J. Robotics Res.* 39, 1525–1548. doi:10.1177/0278364920957090
- Burgués, J., Hernández, V., Lilienthal, A., and Marco, S. (2019). Smelling Nano Aerial Vehicle for Gas Source Localization and Mapping. *Sensors* 19, 478. doi:10.3390/s19030478
- Burgués, J., and Marco, S. (2020). Environmental Chemical Sensing Using Small Drones: A Review. *Sci. Total Environ.* 748, 141172. doi:10.1016/j.scitotenv.2020.141172
- Chiodini, G., Cioni, R., Guidi, M., Raco, B., and Marini, L. (1998). Soil CO₂ Flux Measurements in Volcanic and Geothermal Areas. *Appl. Geochem.* 13, 76. doi:10.1016/S0883-2927(97)00076-0
- Chung, S.-J., Paranjape, A. A., Dames, P., Shen, S., and Kumar, V. (2018). A Survey on Aerial Swarm Robotics. *IEEE Trans. Robot.* 34, 837–855. doi:10.1109/tro.2018.2857475
- Crisp, D., Pollock, H. R., Rosenberg, R., Chapsky, L., Lee, R. A. M., Oyafuso, F. A., et al. (2017). The On-Orbit Performance of the Orbiting Carbon Observatory-2 (OCO-2) Instrument and its Radiometrically Calibrated Products. *Atmos. Meas. Tech.* 10, 59–81. doi:10.5194/AMT-10-59-2017
- Dang, T., Tranzatto, M., Khattak, S., Mascari, F., Alexis, K., and Hutter, M. (2020). Graph-based Subterranean Exploration Path Planning Using Aerial and Legged Robots. *J. Field Robotics* 37, 1363–1388. doi:10.1002/rob.21993
- Diaz, J. A., Pieri, D., Arkin, C. R., Gore, E., Griffin, T. P., Fladeland, M., et al. (2010). Utilization of *In Situ* Airborne MS-based Instrumentation for the Study of Gaseous Emissions at Active Volcanoes. *Int. J. Mass Spectrom.* 295, 105–112. doi:10.1016/j.ijms.2010.04.013
- Diaz, J. A., Pieri, D., Wright, K., Sorensen, P., Kline-Shoder, R., Arkin, C. R., et al. (2015). Unmanned Aerial Mass Spectrometer Systems for *In-Situ* Volcanic Plume Analysis. *J. Am. Soc. Mass. Spectrom.* 26, 292–304. doi:10.1007/S13361-014-1058-X
- Ericksen, J., Aggarwal, A., Fricke, G. M., and Moses, M. E. (2020). LoCUS: A Multi-Robot Loss-Tolerant Algorithm for Surveying Volcanic Plumes. *Proc. - 4th IEEE Int. Conf. Robot. Comput. IRC 2020*, 113–120. doi:10.1109/IRC.2020.00025
- Fischer, T. P., and Aiuppa, A. (2020). AGU Centennial Grand Challenge: Volcanoes and Deep Carbon Global CO₂ Emissions from Subaerial Volcanism-Recent Progress and Future Challenges. *Geochem. Geophys. Geosyst.* 21, 8690. doi:10.1029/2019GC008690
- Fischer, T. P., Arellano, S., Carn, S., Aiuppa, A., Galle, B., Allard, P., et al. (2019). The Emissions of CO₂ and Other Volatiles from the World's Subaerial Volcanoes. *Sci. Rep.* 9, 54682. doi:10.1038/s41598-019-54682-1
- Fischer, T. P., and Lopez, T. M. (2016). First Airborne Samples of a Volcanic Plume for $\delta^{13}\text{C}$ of CO₂ determinations. *Geophys. Res. Lett.* 43, 3272–3279. doi:10.1002/2016GL068499
- Fricke, G. M., Hecker, J. P., Griego, A. D., Tran, L. T., and Moses, M. E. (2016). "A Distributed Deterministic Spiral Search Algorithm for Swarms," in 2016 IEEE/RSJ International Conference on Intelligent Robots and Systems (IROS) (IEEE), 4430–4436. doi:10.1109/IROS.2016.7759652
- Goff, F., and Janik, C. J. (2002). Gas Geochemistry of the Valles Caldera Region, New Mexico and Comparisons with Gases at Yellowstone, Long Valley and Other Geothermal Systems. *J. Volcanology Geothermal Res.* 116, 222. doi:10.1016/S0377-0273(02)00222-6
- Golla, J. (2019). Natural Salinization of the Jemez River, New Mexico: An Insight from Trace Element Geochemistry. *Earth Planet. Sci. ETDs*.
- Gomez, C., and Purdie, H. (2016). UAV- Based Photogrammetry and Geocomputing for Hazards and Disaster Risk Monitoring - A Review. *Geoenvironmental Disasters* 3, 1–11. doi:10.1186/S40677-016-0060-Y/FIGURES/5
- Ihank, T., Fischer, T. P., Kyle, P., Curtis, A., Lee, H., and Sano, Y. (2019). Modification of Fumarolic Gases by the Ice-Covered Edifice of Erebus Volcano, Antarctica. *J. Volcanology Geothermal Res.* 381, 119–139. doi:10.1016/J.JVOLGEORES.2019.05.017
- James, M. R., Carr, B. B., D'Arcy, F., Diefenbach, A. K., Dietterich, H. R., Fornaciai, A., et al. (2020). Volcanological Applications of Unoccupied Aircraft Systems (UAS): Developments, Strategies, and Future Challenges. *Volcanica* 3 67–114. doi:10.30909/vol.03.01.67114
- Johnson, M. S., Schwandner, F. M., Potter, C. S., Nguyen, H. M., Bell, E., Nelson, R. R., et al. (2020). Carbon Dioxide Emissions during the 2018 Kilauea Volcano Eruption Estimated Using OCO-2 Satellite Retrievals. *Geophys. Res. Lett.* 47, e2020GL090507. doi:10.1029/2020GL090507
- Koenig, N., and Howard, A. (2004). "Design and Use Paradigms for Gazebo, an Open-Source Multi-Robot Simulator," in IEEE/RSJ International Conference on Intelligent Robots and Systems (IROS), Sendai, Japan, 28 Sept.-2 Oct. 2004 (IEEE). doi:10.1109/iros.2004.13897273
- Lee, H., Muirhead, J. D., Fischer, T. P., Ebinger, C. J., Kattenhorn, S. A., Sharp, Z. D., et al. (2016). Massive and Prolonged Deep Carbon Emissions Associated with continental Rifting. *Nat. Geosci.* 9 (2 9), 145–149. doi:10.1038/ngeo2622
- Liu, E. J., Aiuppa, A., Alan, A., Arellano, S., Bitetto, M., Bobrowski, N., et al. (2020). Aerial Strategies advance Volcanic Gas Measurements at Inaccessible, Strongly Degassing Volcanoes. *Sci. Adv.* 6, abb9103. doi:10.1126/sciadv.abb9103
- Manga, M., Carn, S. A., Cashman, K. V., Clarke, A. B., Connor, C. B., Cooper, K. M., et al. (2017). Volcanic Eruptions and Their Repose, Unrest, Precursors, and Timing. *Volcanic Eruptions and Their Repose, Unrest, Precursors, and Timing* 1–122, 24650. doi:10.17226/24650
- Neal, C. A., Brantley, S. R., Antolik, L., Babb, J. L., Burgess, M., Calles, K., et al. (2019). The 2018 Rift Eruption and summit Collapse of Kilauea Volcano. *Science* 363, 367–374. doi:10.1126/science.aav7046
- Quigley, M., Conley, K., Gerkey, B., Faust, J., Foote, T., Leibs, J., et al. (2009). "ROS: an Open-Source Robot Operating System," in ICRA workshop on open source software, Kobe, Japan 3, 5
- Radoglou-Grammatikis, P., Sarigiannidis, P., Lagkas, T., and Moscholios, I. (2020). A Compilation of UAV Applications for Precision Agriculture. *Computer Networks* 172, 107148. doi:10.1016/J.COMNET.2020.107148
- Rahilly, K. E. (2020). "Diffuse Flux and Carbon Isotope Composition of Carbon Dioxide Emitted from Valles Caldera, Yellowstone Caldera, and Southwestern Utah Geothermal Sites." Ph.D. thesis (Albuquerque: University of New Mexico).
- Reynolds, C. W. (1987). Proceedings of the 14th Annual Conference on Computer Graphics and Interactive Techniques - SIGGRAPH '87. *Proc. 14th Annu. Conf. Comput. graphics interactive Tech. - SIGGRAPH '87*, 21. doi:10.1145/37401
- Rossi, M., Brunelli, D., Adami, A., Lorenzelli, L., Menna, F., and Remondino, F. (2014). "Gas-drone: Portable Gas Sensing System on UAVs for Gas Leakage Localization," in *SENSORS, 2014 IEEE* (IEEE), 1431–1434. doi:10.1109/icsens.2014.6985282
- Shah, K., Ballard, G., Schmidt, A., and Schwager, M. (2020). Multidrone Aerial Surveys of Penguin Colonies in Antarctica. *Sci. Robot.* 5, 3000. doi:10.1126/SCIROBOTICS.ABC3000
- Stix, J., de Moor, J. M., Rüdiger, J., Alan, A., Corrales, E., D'Arcy, F., et al. (2018). Using Drones and Miniaturized Instrumentation to Study Degassing at Turrialba and Masaya Volcanoes, Central America. *J. Geophys. Res. Solid Earth* 123, 6501–6520. doi:10.1029/2018JB015655
- Stix, J., and de Moor, J. M. (2018). Understanding and Forecasting Phreatic Eruptions Driven by Magmatic Degassing. *Earth Planets Space* 70, 855. doi:10.1186/s40623-018-0855-z
- Stockie, J. M. (2011). The Mathematics of Atmospheric Dispersion Modeling. *SIAM Rev.* 53, 349–372. doi:10.1137/10080991X
- Sun, X., Ansari, N., and Fierro, R. (2020). Jointly Optimized 3D Drone Mounted Base Station Deployment and User Association in Drone Assisted Mobile Access Networks. *IEEE Trans. Vehicular Technol.* 69. doi:10.1109/tvt.2019.2961086

- Thakur, D., Loianno, G., Liu, W., and Kumar, V. (2020). "Nuclear Environments Inspection with Micro Aerial Vehicles: Algorithms and Experiments," in Springer Proceedings in Advanced Robotics (Springer). doi:10.1007/978-3-030-33950-0_1711
- Vásárhelyi, G., Virágh, C., Somorjai, G., Tarcai, N., Szörényi, T., Nepusz, T., et al. (2014). "Outdoor Flocking and Formation Flight with Autonomous Aerial Robots," in IEEE International Conference on Intelligent Robots and Systems, Chicago, IL, USA, 4-18 Sept. 2014. doi:10.1109/IROS.2014.6943105
- Weber, T. R. (1995). An Analysis of Lemmings: A Swarming Approach to Mine Countermeasures in the VSW/SZ/BZ. Tech. rep., DTIC Document.
- Wood, K., Liu, E. J., Richardson, T., Clarke, R., Freer, J., Aiuppa, A., et al. (2020). BVLOS UAS Operations in Highly-Turbulent Volcanic Plumes. *Front. Robot. AI* 7, 549716. doi:10.3389/frobt.2020.549716

Conflict of Interest: Author SN was employed by the company NV5.

The remaining authors declare that the research was conducted in the absence of any commercial or financial relationships that could be construed as a potential conflict of interest.

Publisher's Note: All claims expressed in this article are solely those of the authors and do not necessarily represent those of their affiliated organizations, or those of the publisher, the editors and the reviewers. Any product that may be evaluated in this article, or claim that may be made by its manufacturer, is not guaranteed or endorsed by the publisher.

Copyright © 2022 Ericksen, Fricke, Nowicki, Fischer, Hayes, Rosenberger, Wolf, Fierro and Moses. This is an open-access article distributed under the terms of the Creative Commons Attribution License (CC BY). The use, distribution or reproduction in other forums is permitted, provided the original author(s) and the copyright owner(s) are credited and that the original publication in this journal is cited, in accordance with accepted academic practice. No use, distribution or reproduction is permitted which does not comply with these terms.